

# Directionally tunable and mechanically deformable ferroelectric crystals from rotating polar globular ionic molecules

Jun Harada<sup>1,2\*</sup>, Takafumi Shimojo<sup>2</sup>, Hideaki Oyamaguchi<sup>2</sup>, Hiroyuki Hasegawa<sup>1</sup>, Yukihiro Takahashi<sup>1,2</sup>, Koichiro Satomi<sup>3</sup>, Yasutaka Suzuki<sup>3</sup>, Jun Kawamata<sup>3</sup> & Tamotsu Inabe<sup>1,2\*</sup>

<sup>1</sup>Department of Chemistry, Faculty of Science, Hokkaido University, Sapporo 060-0810, Japan.

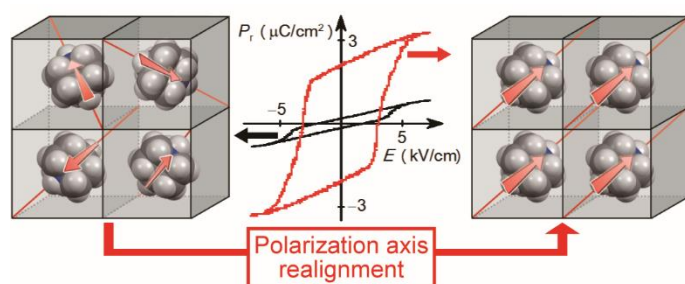
<sup>2</sup>Graduate School of Chemical Sciences and Engineering, Hokkaido University, Sapporo 060-0810, Japan. <sup>3</sup>Graduate School of Medicine, Yamaguchi University, Yamaguchi 753-8512, Japan.

\*e-mail: junharada@sci.hokudai.ac.jp; inabe@sci.hokudai.ac.jp

## Abstract

Ferroelectrics have found a wide range of applications including memory elements, capacitors, and sensors. Molecular ferroelectric crystals have recently attracted growing interest as viable alternatives for conventional ceramic ferroelectrics, especially due to their non-toxicity and solution processability. Herein, we show that a class of molecular compounds known as plastic crystals can exhibit ferroelectricity, provided that the constituent molecules are judiciously chosen from polar ionic molecules. The intrinsic features of plastic crystals, *e.g.* the rotational motion of molecules and phase transitions with lattice symmetry changes, provide the crystals with unique ferroelectric properties relative to conventional molecular crystals, *i.e.* the possibility to flexibly alter the direction of the polarization axis of a grown crystal by applying an electric field. Owing to the tunability of the crystal orientation together with mechanical deformability, this novel type of molecular crystals represents an attractive functional material, which will undoubtedly find diverse applications.

## Graphical Abstract



## Main text

Ferroelectrics exhibit spontaneous electric polarization, the direction of which can be reversed by inverting the external electric field<sup>1</sup>. Ferroelectric crystals do not only exhibit such a switchable polarity, which can be useful in memory elements, but also pyroelectricity, piezoelectricity, and optical second harmonic generation, and for all of these properties technical applications have been developed. Although the majority of ferroelectric materials studied so far are inorganic oxides such as barium titanate and lead zirconium titanate, remarkable progress has recently been achieved in the development of ferroelectric crystals based on molecular compounds<sup>2-9</sup>, including charge-transfer complexes, organic salts, hydrogen-bonded complexes, and alternating  $\pi$ -bond systems exhibiting proton tautomerism. In addition to their obvious non-toxicity (lead-free) and cost efficiency, organic ferroelectrics are also easily deposited in the form of thin films on flexible substrates by solution methods such as spin-coating and printing techniques<sup>10,11</sup>. Yet both the control over crystal orientations and polarization directions of such molecular ferroelectric crystals still represent major challenges for practical applications. The switchable electric polarization in ferroelectric crystals manifests along the direction corresponding to the vector sum of all the molecular dipoles, which is often parallel to the polar axis of the crystal. On account of the low symmetry of their crystal lattices, each grain of molecular ferroelectric crystals can be polarized only in one direction, which is determined at the time of crystal growth. If ferroelectric crystals are grown in orientations or shapes that are unfavourable for the application of an electric field, they cannot develop their ferroelectric properties effectively. The control of crystal orientations is especially important for thin solid films, in most of which the microcrystalline grains aggregate on substrates with randomly or even unfavourably distributed orientations. Without appropriate control of the crystal orientation, only a small portion of the microcrystals can be subjected to effective polarization switching, and the whole sample tends to show a very weak electric polarization, which is distributed unevenly. The restricted orientational control over molecular crystals has so far severely limited their applications in

electronic devices in general. This is in stark contrast to perovskite oxides, where the polarization of crystals can be reoriented by application of a strong electric field (poling). This very feature renders perovskite ceramics, *i.e.* polycrystalline agglomerates, the most industrially valuable ferroelectric and piezoelectric materials. Here, we present a highly promising solution to this problem for molecular ferroelectric crystals: a ferroelectric molecular crystal, whose polarization axis can be easily changed to the desired direction through the rotation of the constituent ionic molecules of the crystal.

Molecular motion in crystals has been studied in various fields of chemistry<sup>12-14</sup>, and the modulation of macroscopic material functions by molecular motions in crystals has recently received particular attention. Changes in the molecular orientation in a semiconductor crystal, for example, were observed to induce a switching of the transfer characteristics of a field-effect transistor<sup>15</sup>. Moreover, the freezing of the pedal motion in crystals was reported to affect the mobility and resistivity of the materials<sup>16,17</sup>. In addition, the rotation of polar molecules in crystals gives rise to dielectric properties<sup>18,19</sup>. Therefore, the reorientation of polar molecules in response to an applied electric field can be a simple design approach to ferroelectric molecular crystals<sup>20</sup>. However, in order to induce resulting ferroelectricity, the polar molecules have to be arranged in their crystals in a way so that their dipole moments do not cancel each other out, and the crystals have to belong to a polar space group. Moreover, not only the orientation of each molecule, but also the whole crystal structure has to be inverted upon reversing the electric field. So far, the development of molecular ferroelectric crystals is severely limited by the difficulties in exerting control over crystal structures to meet these requirements. We have found that plastic crystals composed of polar molecules can form a new class of ferroelectric crystals, the ferroelectricity of which is induced by the rotation of the polar molecules.

The plastic crystal phase is a mesophase between the solid and liquid states, which is found in a large number of compounds with globular molecular structure, *e.g.* adamantane, tetrachloromethane,

and cyclohexane<sup>21,22</sup>. Most of the crystals in plastic phases belong to the cubic crystal system with the highest symmetry point group  $O_h$ , where the molecules exhibit rotator motions<sup>23</sup> and the orientational order of the molecules is lost as in the liquid. Plastic crystals usually undergo one or more solid-solid phase transitions upon cooling to crystal phases with lower lattice symmetry, where the orientation of molecules shows some degree of order. In addition to being of fundamental scientific interest, organic ionic plastic crystals (OIPCs) have recently attracted considerable interest as solid-state electrolytes on account of their high ionic conductivity and good interfacial contact with the electrodes, due to the favourable deformable mechanical properties inherent to plastic crystals<sup>24–26</sup>. In this paper we will show that ionic plastic crystals can also be ferroelectric crystals, by demonstrating that a new ionic molecular crystal, quinuclidinium perrhenate (**1**), exhibits ferroelectricity above room temperature and undergoes a phase transition to a plastic crystal phase at higher temperature. The phase transition between ferroelectric and plastic phases involves changes of the crystal lattice symmetry, which allowed a facile modification of the crystal orientation and the direction of the polarization axis by application of an electric field.

## Results and discussion

**Preparation and phase transitions.** A simple neutralization reaction between the commercially available organic amine 1-azabicyclo[2.2.2]octane (quinuclidine) and perrhenic acid furnished the crystalline salt **1**. The quinuclidinium cation has spherical geometry, and its dipole moment ( $\mu = 3.1$  D calculated at the MP2/6-31+G\* level of theory) is aligned in parallel to the 3-fold axis, while the perrhenate anion exhibits a nonpolar tetrahedral structure (Fig. 1a). Phase transitions of the crystals and accompanying crystal symmetry changes were examined by differential scanning calorimetry (DSC) and optical second harmonic generation (SHG) measurements (Supplementary Fig. S1). As usually observed for crystals exhibiting plastic phases, crystals of **1** showed solid-solid phase transitions, two of which were observed in the DSC traces at ca. 345 and 367 K. We will hereafter

refer to the three solid phases, separated by the two phase transitions, as the low temperature phase (LTP), the intermediate temperature phase (ITP), and the high temperature phase (HTP). Non-zero values of the intensity of the SHG in the LTP decreased to some extent in the ITP, before falling to zero in the HTP, which clearly shows that the crystal structures in the LTP and ITP are non-centrosymmetric, while that in the HTP is centrosymmetric. The higher-temperature phase transition at 367 K (ITP/HTP) is therefore consistent with a ferroelectric phase transition: a polar non-centrosymmetric structure in the low temperature ferroelectric phase changes to a nonpolar centrosymmetric structure in the high temperature paraelectric phase.

**Crystal structures.** The crystal structures and their changes at the phase transitions were examined by X-ray diffraction analysis. The crystal and experimental data are summarized in Supplementary Table S1. The details of the space group assignment and the crystal lattice transformations at the phase transitions are described in Supplementary Discussion. At room temperature (LTP), **1** crystallizes in the orthorhombic crystal system ( $a = 8.9571(9)$ ,  $b = 5.9973(6)$ ,  $c = 9.1546(9)$  Å at 300 K) with the non-centrosymmetric space group  $Pmn2_1$  (Fig. 1b). Both molecular ions at each crystal site adopt only one orientation. The orthorhombic crystal in the LTP was transformed to the trigonal crystal system in the ITP, which possesses a pseudo-cubic rhombohedral unit cell ( $a = 6.360(2)$  Å,  $\alpha = 89.912(3)^\circ$  at 350 K) with the non-centrosymmetric space group  $R3m$ . The final phase transition to the HTP was associated with structural changes to the cubic crystal system ( $a = 6.388(1)$  Å at 380 K) and the centrosymmetric space group  $Pm\bar{3}m$ . Thus, the crystallographic point group changed from  $C_{2v}$  to  $C_{3v}$  and finally to  $O_h$ . In the ITP and HTP, the orientations of both the molecular cations and anions were disordered (Supplementary Fig. S2). The totally disordered molecular structures and the cubic crystal system with the CsCl-type structure strongly suggest that the HTP is the plastic crystal phase, where the molecules undergo an isotropic rotator motion.

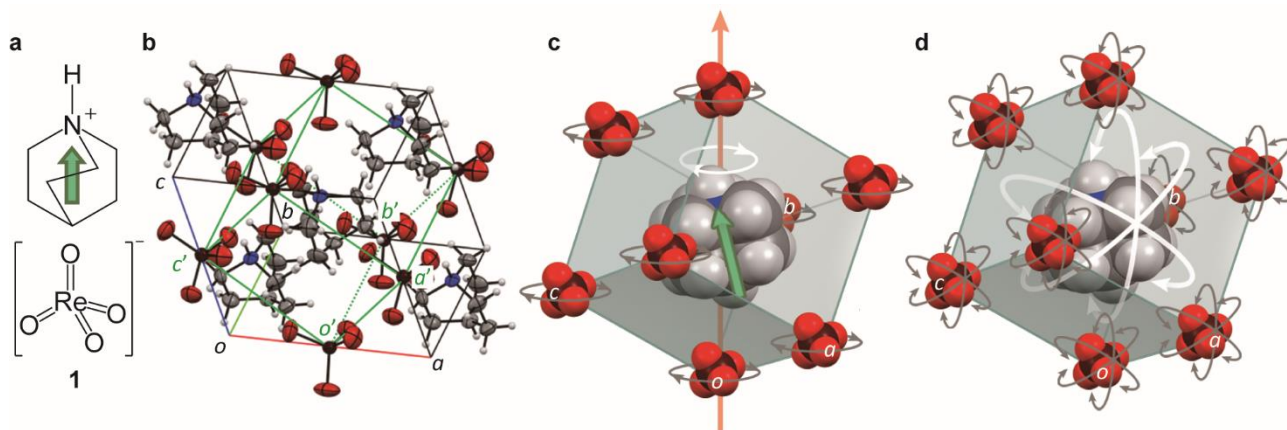


**Figure 1 | Molecular and crystal structures.** **a**, The dipole moment of the quinuclidinium cation is indicated by the green arrow. **b**, The crystal structure in the LTP (300 K). The pseudo-cubic unit cell corresponding to that in the ITP and HTP is outlined in green. **c**, Schematic illustration of the crystal structure in the ferroelectric phase (ITP) and rotational motions therein. The red arrow indicates the spontaneous polarization of the crystal along the polar 3-fold axis. The green arrows indicate the dipole moment of the disordered cation. **d**, Schematic illustration of the plastic crystal phase (HTP) and isotropic rotator motions therein.

Although only limited information was available for the crystal structures in the ITP and HTP, due to the severe rotational disorders of both cation and anion, we can still envision the following features schematically illustrated in Fig. 1c–d (for a detailed discussion, see Supplementary Discussion). In the rhombohedral cell of the ITP, the nitrogen atom of the quinuclidinium cation resides on the 3-fold disordered sites generated by the crystallographic 3-fold axis in the [111] direction. The molecular axis of the polar cation is slightly tilted away from the 3-fold axis, which indicates that the cage-like cation undergoes a precession movement, as well as a rotational motion about the molecular axis. In the cubic crystal (HTP), additional rotational degrees of freedom including an inversion of the electric dipole of the cation allow the molecules to rotate isotropically at the crystal site.

**Ferroelectric properties.** In the ITP, crystals of **1** exhibited ferroelectric behaviour. The dielectric constant shown in Fig. 2a, which depicts the real part ( $\epsilon'$ ) of the complex dielectric constant as a function of temperature, displayed a sharp peak characteristic of ferroelectric transitions (Curie temperature  $T_c = 367$  K). Above  $T_c$ , the  $\epsilon'$  values obeyed the Curie–Weiss law,  $\epsilon' = C/(T - \theta)$ . The Curie–Weiss temperature ( $\theta = 365$  K) and the Curie constant ( $C = 2.4 \times 10^3$  K) were deduced from the linear fitting of the  $1/\epsilon' - T$  relationship. The polarization–electric field ( $P$ – $E$ ) diagrams (Fig. 2b) exhibited well-defined rectangular hysteresis loops in the temperature range between 345 and 367 K, which clearly shows that the ionic crystals are ferroelectric in the ITP. In spite of its polar crystal structure, the LTP did not exhibit any ferroelectric behaviour under the present experimental conditions. This behaviour is similar to the nonpolar HTP, and may be attributed to the presence of a large coercive field in the LTP. According to the structural changes of the crystal at the ferroelectric transition, the ferroelectricity can be interpreted in terms of rotational motion of the polar quinuclidinium ion. The remanent polarization,  $P_r$ , and the coercive field,  $E_c$ , which represents the minimum electric field required for an inversion of the polarization, were determined from the intercepts in the  $P$ – $E$  hysteresis loops ( $P_r$  at  $E = 0$  and  $E_c$  at  $P = 0$ ) as a function of temperature (Fig. 2c). The reasonably large  $P_r$  values, typically  $3.5 \mu\text{C cm}^{-2}$  at 345 K, are comparable to that of a typical molecular ferroelectric crystal such as triglycine sulfate (TGS;  $3.8 \mu\text{C cm}^{-2}$ )<sup>2</sup>. The  $E_c$  values, which range from 2 to 5  $\text{kV cm}^{-1}$ , depending on the temperature, are much smaller than those of the ferroelectric poly(vinylidene) difluoride (PVDF) family ( $\sim 500 \text{ kV cm}^{-1}$ )<sup>2</sup>.

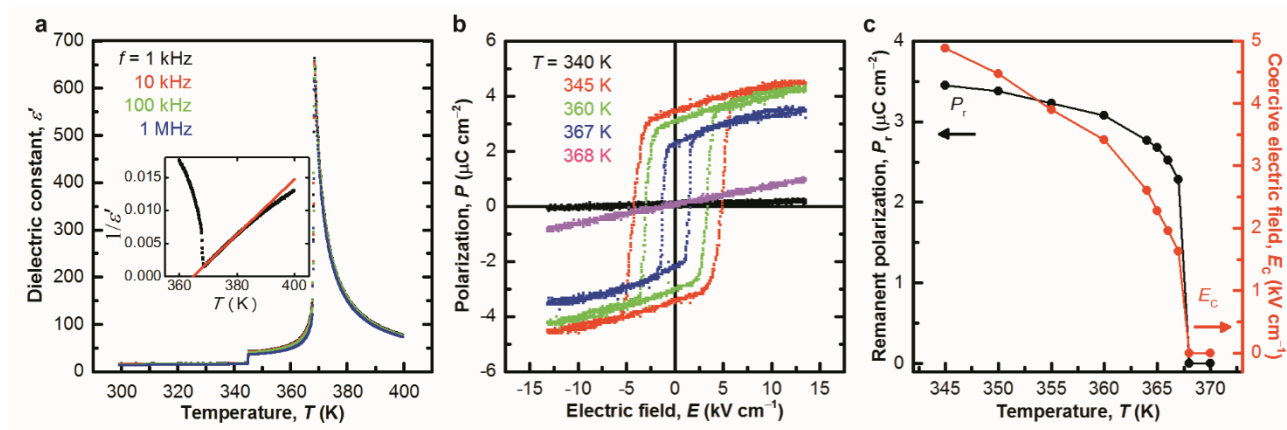


**Figure 2 | Ferroelectric properties.** **a**, The dielectric constant,  $\epsilon'$ , measured as a function of temperature at various frequencies along the [111] direction of the unit cell of the LTP. The inset shows a linear fit to the Curie–Weiss law using  $\epsilon'$  at 1 kHz. **b**, Hysteresis loops of the electric polarization measured with an a.c. electric field of 10 Hz applied in parallel to the  $a$ -axis of the unit cell of the LTP. **c**, Temperature dependence of the remanent polarization,  $P_r$ , and coercive field,  $E_c$ , obtained from  $P$ – $E$  hysteresis loops measured under the same conditions as for **b**.

The ferroelectricity of the crystal of **1** showed both high frequency performance and fatigue resistance (Supplementary Fig. S3). The ferroelectric polarization was switchable up to frequencies of 2 kHz, which was the highest frequency limit of our measurements, whereby only a marginal decrease of the  $P_r$  values was observed. The fast polarization switching demonstrates that the crystal can be categorized as a highest-speed response molecule-based ferroelectric crystal<sup>27</sup>. This ferroelectric crystal moreover exhibited high fatigue resistance, and the  $P$ – $E$  hysteresis loop did not show any signs of deterioration, even after  $10^5$  cycles of polarization switching. The high frequency and fatigue resistance of ferroelectric switching, as well as the low  $E_c$  values are probably attributable to the polarization inversion through almost frictionless molecular rotation.

**Changes in crystal orientation.** Owing to the presence of the plastic crystal phase at higher temperatures, ferroelectric crystals of **1** are endowed with unique features that are highly desirable,

especially for device fabrication. One of these highly desirable features is mechanical plasticity, which will be discussed in a later section, while another is that the direction of the electric polarization axis can be changed in three dimensions without having to reconstruct the crystal. This directional tunability of the polarization axis is attributed to the phase transition from a high-temperature phase that has typically cubic lattice symmetry in plastic crystals, to a low-temperature phase with lower lattice symmetry (*vide infra*).

Upon the phase change of an as-grown crystal of **1** from the LTP to the ferroelectric ITP, the direction of the polar axis of each unit cell is uniformly aligned in the crystal, which generates electrical polarization in the same direction (Fig. 3a). The polarity of the crystal can also be reversed by application of an electric field (Fig. 3b). Most molecular ferroelectric crystals exhibit uniaxial polarization due to their low crystal symmetry, and the 180° flipping is the only allowed directional change of the polarization. Like most plastic crystals, the crystal of **1** in the HTP belongs to the cubic crystal system, where the four body diagonals are equivalent 3-fold axes. Rotator motions and orientational disorders of the polar quinuclidinium ions result in a non-polar crystal structure of the plastic phase (Fig. 3c). The transition from the HTP to the ITP reduces the crystal symmetry, and only one of the four axes becomes the 3-fold axis of the rhombohedral lattice, which coincides with the ferroelectric polarization axis. Phase transitions associated with the reduction of lattice symmetry usually entail crystal twinning, and the resulting crystal represents an aggregate of multiple domains with identical unit cells in different orientations<sup>28-29</sup>. After the transition from the HTP to the ITP, the rhombohedral crystal in the ITP consists of twinned domains, and the 3-fold axis of each domain is randomly taken from the four 3-fold axes of the cubic lattice (Fig. 3d). Accordingly, the transitions between the ferroelectric (ITP) and the plastic phase (HTP) eliminate the direction, along which the polar axis of the as-grown crystal was aligned. As an exceedingly important aspect of this system, exhibiting both a ferroelectric and a plastic crystal phase with cubic crystal system, the original orientation of an as-grown crystal can be changed in a specific direction by application of an electric

field during the transition from the HTP to the ITP (field-cooling), which can realign the polarization axes (Fig. 3e). Accordingly, the entire crystal or each domain then chooses its new polar 3-fold axis from the four possible 3-fold axes selectively, while it chooses its axis randomly in the absence of an electric field. In the presence of an electric field, the energetically most favourable axis is selected, and the polarization of the crystal is aligned closely with the electric field. The resulting crystal, with a realigned polar axis, exhibits a spontaneous polarization in a direction different from that of the as-grown crystal, and the polarity of the crystal can be switched by the electric field (Fig. 3f). Thus, the orientation of the crystal can be changed via the phase transitions without destroying the crystal, and the direction of the polar axis can be tuned to align in a direction favourable for the ferroelectric switching conducted by electrodes with fixed orientations.

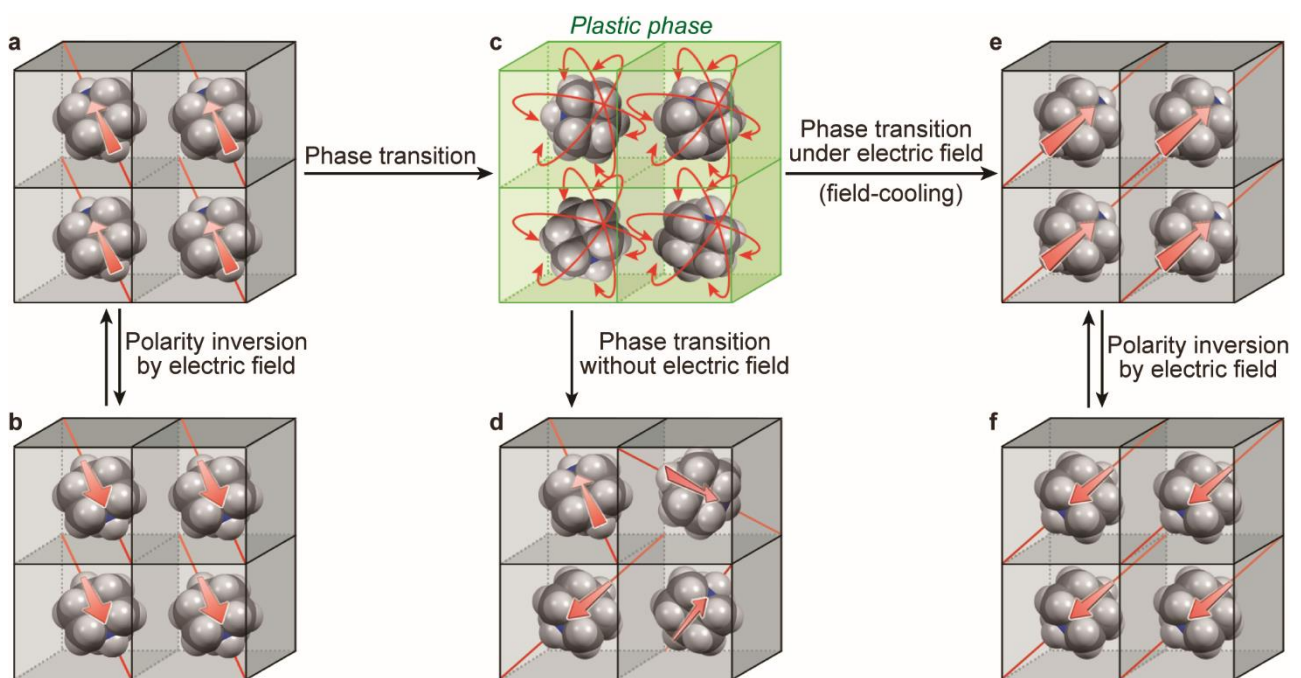


**Figure 3 | Direction of the crystal orientation.** **a**, The ferroelectric phase (ITP) of an as-grown crystal. **b**, The polarity of the crystal can be inverted by application of an electric field. **c**, The plastic crystal phase (HTP). **d**, The ferroelectric phase (ITP) generated by the phase transition from the HTP in the absence of an electric field. **e**, The ferroelectric phase (ITP) generated by the transition from the HTP in the presence of an electric field (field-cooling). The polarization axis of this crystal differs from that of the as-grown crystal (**a**). **f**, The polarity of the crystal can be inverted by

application of an electric field.

**Polarization enhancement by realignment of polar axes.** The realignment of the polar axes in crystals was confirmed by  $P$ - $E$  hysteresis experiments using a powder sample of **1**. Before the electrical realignment of the polar axes, a compaction pellet of microcrystalline powder of **1** provided a  $P$ - $E$  hysteresis loop (black loop in Fig. 4a) with a  $P_r$  value of  $0.2 \mu\text{C cm}^{-2}$  at 365 K, which is much smaller than that of a single crystal at the same temperature ( $2.7 \mu\text{C cm}^{-2}$ ). This clearly reflects the random orientation of microcrystalline grains in the pellet and/or resulting immobilized domain walls<sup>30</sup>. Subsequently, the sample was heated to the HTP, before being field-cooled to the ITP under application of a 10 Hz a.c. electric field ( $E_{\text{max}} = 7.1 \text{ kV cm}^{-1}$ ). As a result, the  $P_r$  value increased dramatically to  $2.1 \mu\text{C cm}^{-2}$  (red loop in Fig. 4a), which is comparable to that of the single crystal, thus demonstrating the polarization enhancement through the electrical realignment of the polar axes of the microcrystalline grains. This large  $P_r$  value reverted to the original small value after annealing, *i.e.* exposing the pellet to a cycle of transitions between the ITP and the HTP in the absence of an electric field (green loop in Fig. 4a), which resulted in a random orientation of the polar axis of each grain tantamount to a loss of any favourable alignment. Supplementary Fig. S4 shows a schematic illustration of the changes in the domain structures, which accompany the phase transitions under different conditions.

Furthermore, the polar axis of the crystal can also be realigned in the ferroelectric phase by applying a slightly larger electric field than that required for the realignment during the phase transition (Fig. 4b-c). After annealing of the crystalline powder of **1** by phase transitions in the absence of an electric field, a small polarization was observed at 365 K with a 10 Hz a.c. electric field ( $E_{\text{max}} = 7.1 \text{ kV cm}^{-1}$ ; black loop in Fig. 4b). The small value of  $P_r$  indicated that the polar axes of the crystal grains did not realign in the ferroelectric phase under the a.c. electric field applied for the measurement, which was identical to that used for the electrical realignment during the phase

transition. The polarization, in contrast, was greatly enhanced by sequentially increasing  $E_{\max}$  values up to  $11 \text{ kV cm}^{-1}$ . Once the polarization was enhanced by electrical alignment of the polar axes of the microcrystals, the enhanced polarization can be switched by significantly smaller electric fields (Fig. 4c). The realignment of polar axes without phase transitions can be explained by the pseudo-cubic symmetry of the rhombohedral lattice of **1** in the ferroelectric phase. Molecular reorientations with small activation energies can easily transform the orientation of the rhombohedral crystal to the one that is energetically most stable under the applied electric field.

The realignment of the polarization axes observed for **1** is essentially identical to the widely used poling process for ferroelectric perovskite ceramics, as it polarizes randomly oriented agglomerates of small crystals in a direction close to the applied strong electric field<sup>31</sup>. The viability of the poling process in perovskite ferroelectrics is responsible for their high practical utility, *i.e.* these materials can be used in the form of polycrystalline ceramics, without the need to grow single crystals with controlled shape and orientation. The results observed for **1** clearly demonstrate directional tunability of the polarization, which means that molecular ferroelectric crystals can share the most valuable feature of ferroelectric perovskites. Although the chemical processes responsible for the reorientation of the polarization in **1** are substantially different from those in perovskites, the highly symmetric crystal structure in the HTP, which belongs to the same point group ( $O_h$ ) as the high-temperature phase of perovskites, renders the poling process applicable even to molecular ferroelectric crystals. Plastic crystals usually belong to the cubic crystal system, which is exceptional for molecular crystals. Plastic crystals exhibiting ferroelectricity in low-temperature phases may therefore find practical applications, similarly to ferroelectric perovskites ceramics, in the form of microcrystalline powders.

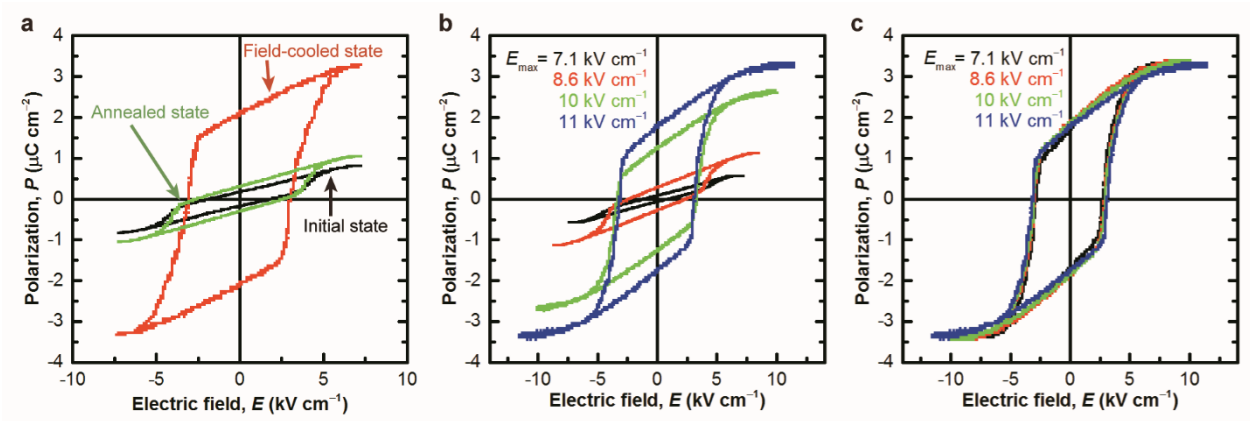


**Figure 4 | Polarization enhancement by application of an electric field.** **a**, Hysteresis loops measured at 10 Hz and 365 K using a compaction pellet of a powder sample of **1**. Black: initial state (prior to electrical realignment), red: field-cooled state (1. heating to the HTP; 2. cooling to the ITP under an a.c. electric field), and green: annealed state (1. heating to the HTP; 2. cooling to the ITP in the absence of an electric field). **b**, Hysteresis loops measured at 365 K by sequentially increasing the maximum value of the applied a.c. electric field,  $E_{\text{max}}$  (10 Hz frequency). **c**, After the measurements shown in **b**, the hysteresis loops were measured at 365 K with sequentially decreasing  $E_{\text{max}}$  (10 Hz frequency). For all the measurements shown in **a–c**, the same sample was used.

**Plastic behaviour of the crystals.** As previously mentioned, another important aspect of the ionic crystal of **1** is its mechanical deformability under pressure, which is inherent to plastic crystals. Scanning electron microscopy (SEM) provided a proof of plastic deformation in the HTP by observing the crystal morphology before and after application of uniaxial pressure (Fig. 5). In contrast to the fractured crystals, which were exposed to pressure at room temperature (LTP), the exposure to pressure at high temperature (HTP) resulted in a plastic deformation of the crystal without fracture. Several other SEM images, supporting the plastic deformation in the HTP, are shown in Supplementary Fig. S5. The observed mechanical plasticity of ferroelectric crystals of **1** will undoubtedly be extremely advantageous in the preparation of ferroelectric thin films suitable for device fabrications.

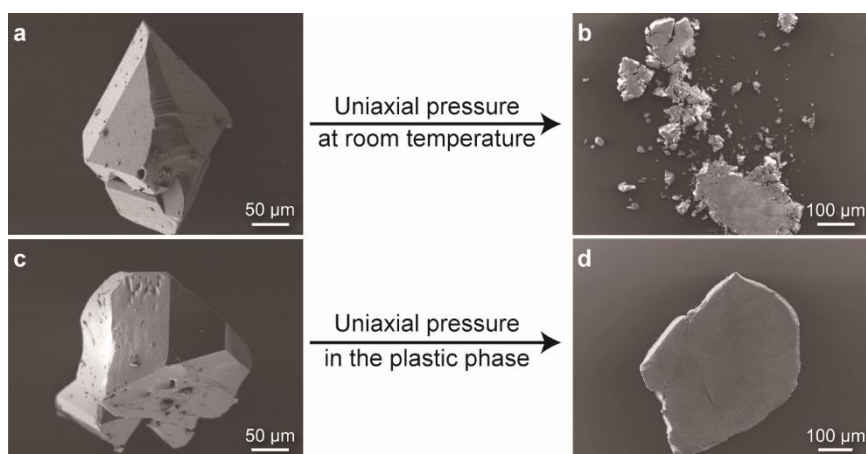


**Figure 5 | Phase-dependent pressure-induced morphology changes of crystals of 1.** **a** and **b**, SEM images of a single crystal of **1** before and after application of uniaxial pressure at room temperature (LTP). **c** and **d**, SEM images of a single crystal of **1** before and after application of uniaxial pressure at high temperature (HTP; plastic crystal phase).

## Conclusions

In summary, we have presented a simple and versatile design principle for ferroelectric molecular crystals. The combination of a globular molecular cation with a tetrahedral anion results in the formation of plastic crystals that show ferroelectricity in the low temperature phase, when at least one of the ions possesses an electric dipole. Unique ferroelectric properties inherent to the presence of a plastic crystal phase were demonstrated for crystals of **1**, which showed directional tunability of the polarization axes and mechanical deformability. In addition to providing a solution to the low dimensionality that ferroelectric molecular crystals have previously encountered, these features are invaluable for practical applications, especially for the fabrication of thin solid films. Deposition of microcrystals on a substrate by a solution process followed by application of pressure and an electric field may thus easily yield pinhole-free thin films with controlled crystal orientations and uniform thickness, which are highly desirable for *e.g.* non-volatile ferroelectric random access memory (FeRAM) devices.

The diversity of ionic plastic crystals that can be readily prepared from globular polar amines

will stimulate the exploration and the development of this type of ferroelectric crystals. To access the unique features encountered for **1**, the crystals have to belong to the cubic crystal system in the high-temperature phase and to exhibit the ferroelectric phase transition associated with the reduction of the crystal lattice symmetry, similar to perovskite ferroelectric crystals. Although the occurrence of any of these features depends on the crystal structures and is, therefore, difficult to predict with certainty from the molecular structures of a given compound, globular polar molecules that exhibit plastic crystal phases meet most of the requirements: the isotropically rotating molecules that occupy spherical volumes usually crystallize in the highly symmetric cubic lattice. The increase of orientational order of these molecules at low temperature induces solid-solid phase transitions, where the cubic crystal lattice symmetry has to be reduced to match the low symmetry of the ordered molecules. The only remaining condition required for the plastic crystals is the non-centrosymmetric polar crystal structure in the low-temperature phase, which is necessary for ferroelectricity. Although the development of ferroelectric crystal structures still has to be achieved through a trial-and-error approach, derivatives of a known ferroelectric crystalline compound are usually likely to generate ferroelectric crystals. We can, therefore, expect to discover a series of ferroelectric crystals, equipped with the unique features found in **1**, by exploring ionic crystals composed of globular polar molecules.

In fact, we have found that several quinuclidinium salts, *e.g.* quinuclidinium tetrafluoroborate (**2**), quinuclidinium perchlorate (**3**), quinuclidinium hexafluorophosphate (**4**), exhibit one or more solid-solid phase transitions (see Supplementary Fig. S6). Although we have so far been unable to obtain crystals of sufficient quality in order to determine their solid-state structures by single-crystal X-ray diffraction analysis, and although we have not yet identified the details of their phase structures, the powder X-ray diffraction patterns of **2–4** in the high-temperature phase could be indexed and revealed cubic unit cells, which is indicative of plastic crystal phases. Ionic crystals of globular polar molecules can, therefore, be regarded as promising targets for the development of new

ferroelectric materials. In addition, chemical modifications of the constituent ions may improve the performance of the resulting crystalline ferroelectrics: for example, ionic molecules with larger dipole moments will provide crystals with increased spontaneous polarization. Tuning the strength of the intermolecular interactions within the crystals will lead to a modified response to the external electric field or to a wider working-temperature range for the resulting ferroelectrics. The systematic investigation of a wide variety of ionic compounds that can be obtained from the combination of numerous globular polar bases and acids will undoubtedly lead to the development of this type of molecular crystals, which will not only greatly enhance the utility of molecular ferroelectrics, but will also lead to new applications of this unique functional material.

## Methods

**Materials.** Quinuclidinium perrhenate (**1**) was prepared from stoichiometric amounts (1:1) of quinuclidine and perrhenic acid in aqueous ethanol. The white microcrystalline powder of **1** that precipitated from solution upon the addition of diethyl ether was filtered and dried under vacuum. Colourless single crystals used for single crystal X-ray diffraction analysis and electric measurements were grown by the slow evaporation of solvent from ethanol solutions of **1** at room temperature. Powder samples of **2–4** were prepared in a similar fashion, using the corresponding acids.

**Measurements.** DSC measurements were recorded on a Rigaku Thermo Plus DSC8230 with heating/cooling rates of 5 K/min. Microcrystalline samples were weighed and sealed in aluminum pans.

SHG measurements were conducted by using a compaction pellet of microcrystalline powder of **1**. A femtosecond pulsed beam ( $\lambda = 1064$  nm) from an optical parametric amplifier (Spectra-Physics, OPA-800C) pumped by a beam from a Ti:sapphire regenerative amplifier (Spectra-Physics, Spitfire)

was employed as the light source. The pulse duration was typically 150–200 fs, while the repetition rate was 1 kHz, and the average incident power was 0.2 mW. The incident beam was focused using a plano-convex lens ( $f = 120$  mm). The output SHG signals were detected by a photomultiplier tube (Hamamatsu, Model R212) and processed using a boxcar average (Stanford Research, Model SR250). The value of SHG intensity of the sample is expressed as the ratio relative to the SHG intensity of urea powder measured using an identical experimental setup at room temperature.

For the electric measurements, a homemade thermostat was used to control the temperature of the samples under a helium atmosphere between 300 and 400 K. The temperature was measured using a Si diode thermometer mounted on the sample holder. Single crystals or compaction pellets of **1** were used as the samples with electrodes of painted carbon or gold paste. The dielectric constant was measured with an Agilent E4980A precision LCR meter (1 kHz – 1 MHz). The  $P$ – $E$  hysteresis measurements were conducted using a Sawyer-Tower circuit<sup>32</sup> with a high-voltage triangular wave field at various frequencies (10 Hz – 2 kHz). Small contributions of electric conductivity, which distort the hysteresis loops to be rounded and elliptical, were eliminated by adjusting a variable resistor so as to yield compensated hysteresis loops with straight lines in the high-electric field corners.

The morphology of the crystals was characterized at ambient temperature using a JEOL JSM–6700FT field-emission scanning electron microscope (FE–SEM) at an acceleration voltage of 5 kV. All samples were prepared on silicon substrates, and uniaxial pressure was applied to the crystals between a pair of silicon substrates using a hand press for KBr pellets.

Powder X-ray diffraction patterns of microcrystalline powder samples of **1** were measured using a Bruker D8 ADVANCE diffractometer. The diffraction patterns confirmed that the powder samples used for the DSC, SHG, and electric measurements had crystal structures identical to that determined by single-crystal X-ray diffraction analysis at 300 K. High-temperature diffraction patterns for **2–4** were recorded using a variable-temperature stage (Anton Paar TTK 450). The diffraction patterns

were indexed using the DASH 3.3.3 software<sup>33</sup>.

The single-crystal X-ray diffraction analysis was performed on a Bruker APEX II Ultra diffractometer (Mo  $K\alpha$  radiation,  $\lambda = 0.71073$  Å). The temperature of the sample was regulated using a Japan Thermal Engineering DX-CS190LD N<sub>2</sub>-gas-flow cryostat and was calibrated using a thermocouple. Diffraction data were processed with the Bruker Apex2 program suite. Structures were solved by direct methods (SHELXT-2014) and refined by full-matrix least-squares on  $F^2$  using SHELXL-2014<sup>34</sup>. For the LTP crystal structure, all hydrogen atoms were refined using riding models and all non-hydrogen atoms were refined anisotropically. Accurate ITP and HTP molecular crystal structures could not be obtained on account of the severe rotational disorders, and hydrogen atoms were not incorporated in the refinement model. The distinction of carbon and nitrogen atoms in the quinuclidinium cation was impossible in the HTP, and all atoms were refined as carbon atoms. Details of the refinement have been deposited as Crystallographic Information Files embedding the SHELXL-2014 res files. CCDC 1419397 (**1** at 300 K, LTP), 1419398 (**1** at 350 K, ITP) and 1419399 (**1** at 380 K, HTP) contain the supplementary crystallographic data for this paper, and can be obtained free of charge from the Cambridge Crystallographic Data Centre via [www.ccdc.cam.ac.uk/getstructures](http://www.ccdc.cam.ac.uk/getstructures).

## References

1. Lines, M. E. & Glass, A. M. *Principles and Applications of Ferroelectrics and Related Materials* (Oxford University Press, New York, 1977).
2. Horiuchi, S. & Tokura, Y. Organic ferroelectrics. *Nature Mater.* **7**, 357–366 (2008).
3. Tayi, A. S., Kaeser, A., Matsumoto, M., Aida, T. & Stupp, S. I. Supramolecular ferroelectrics. *Nature Chem.* **7**, 281–294 (2015).
4. Tokura, Y. *et al.* Domain-wall dynamics in organic charge-transfer compounds with one-dimensional ferroelectricity. *Phys. Rev. Lett.* **63**, 2405–2408 (1989).

5. Katrusiak, A. & Szafranski, M. Ferroelectricity in NH $\cdots$ N hydrogen bonded crystals. *Phys. Rev. Lett.* **82**, 576–579 (1999).
6. Horiuchi, S. *et al.* Ferroelectricity near room temperature in co-crystals of nonpolar organic molecules. *Nature Mater.* **4**, 163–166 (2005).
7. Horiuchi, S. *et al.* Above-room-temperature ferroelectricity in a single-component molecular crystal. *Nature* **463**, 789–792 (2010).
8. Tayi, A. S. *et al.* Room-temperature ferroelectricity in supramolecular networks of charge-transfer complexes. *Nature* **488**, 485–489 (2012).
9. Fu, D.-W. *et al.* Diisopropylammonium bromide is a high-temperature molecular ferroelectric crystal. *Science* **339**, 425–428 (2013).
10. Ling, M. M. & Bao, Z. Thin film deposition, patterning, and printing in organic thin film transistors. *Chem. Mater.* **16**, 4824–4840 (2004).
11. Gundlach, D. J. *et al.* Contact-induced crystallinity for high-performance soluble acene-based transistors and circuits. *Nature Mater.* **7**, 216–221 (2008).
12. Gavezzotti, A. & Simonetta, M. Crystal chemistry in organic solids. *Chem. Rev.* **82**, 1–13 (1982).
13. Fyfe, C. A. *Solid State NMR for Chemists* (CFC Press, Guelph, 1983).
14. Vogelsberg, C. S. & Garcia-Garibay, M. A. Crystalline molecular machines: function, phase order, dimensionality, and composition. *Chem. Soc. Rev.* **41**, 1892–1910 (2012).
15. Yokokura, S. *et al.* Switching of transfer characteristics of an organic field-effect transistor by phase transitions: Sensitive response to molecular dynamics and charge fluctuation. *Chem. Mater.* **27**, 4441–4449 (2015).
16. Goetz, K. P. *et al.* Freezing-in orientational disorder induces crossover from thermally-activated to temperature-independent transport in organic semiconductors. *Nature Commun.* **5**, 5642 (2014).

17. Harada, J. & Ogawa, K. Pedal motion in crystals. *Chem. Soc. Rev.* **38**, 2244–2252 (2009).
18. Horansky, R. D. *et al.* Dielectric response of a dipolar molecular rotor crystal. *Phys. Rev. B* **72**, 014302 (2005).
19. Harada, J., Ohtani, M., Takahashi, Y. & Inabe, T. Molecular motion, dielectric response, and phase transition of charge-transfer crystals: Acquired dynamic and dielectric properties of polar molecules in crystals. *J. Am. Chem. Soc.* **137**, 4477–4486 (2015).
20. Akutagawa, T. *et al.* Ferroelectricity and polarity control in solid-state flip-flop supramolecular rotators. *Nature Mater.* **8**, 342–347 (2009).
21. Timmermans, J. Plastic crystals: A historical review. *J. Phys. Chem. Solids* **18**, 1–8 (1961).
22. Sherwood, J. N. (ed.) *The Plastically Crystalline State: Orientationally Disordered Crystals* (Wiley, London, 1979).
23. Brand, R., Lunkenheimer, P. & Loidl, A. Relaxation dynamics in plastic crystals. *J. Chem. Phys.* **116**, 10386–10401 (2002).
24. MacFarlane, D. R., Huang, J. & Forsyth, M. Lithium-doped plastic crystal electrolytes exhibiting fast ion conduction for secondary batteries. *Nature* **402**, 792–794 (1999).
25. MacFarlane, D. R. & Forsyth, M. Plastic crystal electrolyte materials: New perspectives on solid state ionics. *Adv. Mater.* **13**, 957–966 (2001).
26. Pringle, J. M., Howlett, P. C., MacFarlane, D. R. & Forsyth, M. Organic ionic plastic crystals: recent advances. *J. Mater. Chem.* **20**, 2056–2062 (2010).
27. Cai, H.-L. *et al.* 4-(Cyanomethyl)anilinium perchlorate: A new displacive-type molecular ferroelectric. *Phys. Rev. Lett.* **107**, 147601 (2011).
28. Giacovazzo, C. (ed.) *Fundamentals of Crystallography*. (Oxford University Press, Oxford, 2002).
29. Parsons, S. Introduction to twinning. *Acta Crystallographica Section D* **59**, 1995–2003 (2003).
30. Kagawa, F. *et al.* Polarization switching ability dependent on multidomain topology in a

- uniaxial organic ferroelectric. *Nano Lett.* **14**, 239–243 (2014).
31. Jaffe, B., Cook Jr., W. R. & Jaffe, H. *Piezoelectric Ceramics* (Academic Press, London and New York, 1971).
  32. Sawyer, C. B. & Tower, C. H. Rochelle salt as a dielectric. *Phys. Rev.* **35**, 269–273 (1930).
  33. David, W. I. F. *et al.* DASH: a program for crystal structure determination from powder diffraction data. *J. Appl. Crystallogr.* **39**, 910–915 (2006).
  34. Sheldrick, G. M. A short history of SHELX. *Acta Crystallogr. Sect. A* **64**, 112–122 (2008).

### **Acknowledgements**

This work was partly supported by JSPS KAKENHI Grant Number 26620054 and a Grant-in-Aid for Scientific Research on Innovative Areas “ $\pi$ -System Figuration: Control of Electron and Structural Dynamism for Innovative Functions” (Grant Number 15H00980) from the Ministry of Education, Culture, Sports, Science and Technology, Japan. The authors would like to thank Dr. Kobayashi (Hokkaido University) for access to a Bruker D8 ADVANCE powder X-ray diffractometer.

### **Author contributions**

J.H. conceived and designed the study, performed the crystallographic studies, and wrote the manuscript; T.S. and H.O. prepared the samples and performed the hysteresis experiments; T.S. carried out the dielectric measurements and thermal analysis; Y.T. assisted with the hysteresis and dielectric experiments; H.H. and H.O. carried out the scanning electron microscopy; K.S., Y.S., and J.K. conducted the SHG measurements; T.I. contributed to the design of the study and supervised the project.

### **Additional information**

Supplementary Information is available in the online version of the paper. Reprints and permissions

information is available online at [www.nature.com/reprints](http://www.nature.com/reprints). Crystallographic Information Files for **1** at 300, 350, and 380 K are available as Supplementary Information. Correspondence and requests for materials should be addressed to J.H. ([junharada@sci.hokudai.ac.jp](mailto:junharada@sci.hokudai.ac.jp)) or T.I. ([inabe@sci.hokudai.ac.jp](mailto:inabe@sci.hokudai.ac.jp)).

### **Competing financial interests**

The authors declare no competing financial interests.